10

Fabrication features of amorphous whispering gallery mode microresonators

© T.S. Tebeneva[1], A.E. Shitikov[1], O.V. Benderov[2], V.E. Lobanov[1], A.V. Rodin[2], I.A. Bilenko[1,3]

[1] Russian Quantum Center, 121205 Moscow, Russia
[2] Moscow Institute of Physics and Technology,
141701 Dolgoprudny, Moscow oblast, Russia
[3] Department of Physics, Moscow State University,
119991 Moscow, Russia

e-mail: tetasia19@gmail.ru

Received February 16, 2024
Revised March 21, 2024
Accepted March 21, 2024

Optical high-quality-factor microresonators with whispering gallery modes are extremely promising for various photonic devices, including for the mid-infrared range applications. This range is of great interest for both fundamental and applied problems due to the presence of the fundamental absorption bands of various molecules — the "fingerprint region". The most promising materials for IR photonics based on optical microresonators are various amorphous materials suitable for mass production of microresonators with high-quality-factor in this range. The paper describes a technique for manufacturing high-quality-factor microresonators from arsenic sulfide (As_2S_3) and fluoride glass (ZBLAN) by melting optical fibers, and also examines various defects that arise during the manufacturing process and suggests methods for eliminating them. It is shown that the presented technique makes it possible to achieve a level of quality factor for microresonators limited by fundamental optical losses in the materials used.

Keywords: Whispering gallery modes optical microresonators, fabrication, fluoride fiber, chalcogenide fiber, quality factor measurements.

DOI: 10.61011/EOS.2024.03.58755.6043-23

Introduction

Optical microresonators with whispering gallery modes (WGMs) attract particular attention due to a combination of small geometric dimensions and low optical losses within a wide spectral range [1–3]. WGM microresonators with high-quality-factor are of great interest for spectroscopy [4,5], optical sensorics [6,7], observations and studies of various nonlinear effects [8–10], production of new laser sources [11–13], and stabilization of laser radiation [14–16]. These microresonators open up enormous prospects for the development of photonic components for biosensing [6,17], precision spectroscopic measurements, and monitoring of various gases [4,18] and the production of stable radiation sources [19,20] operating in the mid-infrared (IR) range. Since the fundamental absorption bands of most molecules are found in this range, it is of particular interest for analytical spectroscopy. Radiation sources with a narrow and stable generation line in this range are extremely scarce at present, which is a limiting factor for the development of mid-IR photonics. One way to solve this problem is to design optical components based on WGM microresonators with a high-quality-factor in the discussed range. The first-priority objective of development of mid-IR photonics is the search for suitable materials with low optical losses in the $2\,\mu$m range. Various crystalline and amorphous materials (silicon [21,22], germanium [23–26], fluorides [27–31], chalcogenides [32,33], tellurites [34,35], etc.) are used for the fabrication of WGM microresonators suited for different tasks and areas of application.

The manufacture of WGM microresonators with a high-quality-factor imposes certain requirements as to the surface quality of resonators; therefore, additional mechanical polishing of the surface is needed in the case of crystalline resonators to minimize losses associated with roughness [36–38]. With amorphous materials, the main fabrication method is melting: glass is heated to a temperature above the glass transition one, and it acquires a spherical shape under the influence of surface tension forces [1,39]. Mechanical polishing of the surface is then not required, which is an advantage over crystalline resonators. To produce resonators with minimum surface roughness from amorphous materials, one needs to choose the optimum process conditions with account for the chemical and physical properties of the glasses used. The choice of a heating element is important for the production of WGM microspheres by melting. A fabrication method with a flow of hot inert gas in a vertical tube used as a heating element was presented in [40,41]. This method helps prevent oxidation. Glass is ground into powder with particles up to $200\,\mu$m in size and introduced into a tube. Lifted by the gas flow and heated to the required temperature, these particles melt and acquire a spherical shape. Another option was discussed in [42], where powdered glass was introduced into high-purity oil

that had a high boiling point (higher than the melting point of the glass used) and a high thermal conductivity coefficient and was heated to the glass transition temperature. These fabrication procedures are specific in being suitable for mass production of amorphous resonators with dimensions up to 200 μm; however, both options require a complex experimental setup and non-trivial technological procedures for cleaning the resonator surface.

CO_2 lasers are used widely to produce amorphous WGM microresonators. It is worth noting that the potential of this method in manufacture of WGM microresonators is virtually limitless, since it allows for the production of microresonators of almost any shape and with high precision. For example, CO_2 laser radiation has been used successfully to fabricate bottle microresonators based on optical fibers [43,44]. A CO_2 laser may also be used efficiently for the manufacture of microrod resonators (made, e.g., from fused quartz [45,46]). A whole class of bottle WGM microresonators touted as the key elements of surface nanoscale axial photonics (SNAP) [48] is also worth noting. These microresonators are fabricated on the surface of optical fibers by modulating their effective radius with sub-angstrom accuracy [47–49]. A specific feature of this method is its suitability for production of a large number of coupled WGM microresonators with high accuracy and predefined spectral parameters. This opens up enormous opportunities for examination of nonlinear effects [50], but one still needs a highly sophisticated experimental setup.

CO_2 laser radiation is also used efficiently for the fabrication of microtoroids [51,52]. It was demonstrated in [53] that a high-energy focused CO_2 laser beam provides an opportunity to combine volumetric and integrated technologies for manufacture of optical elements on a chip. The disadvantage of this method is the evaporation of material from the surface with subsequent deposition of vapor on the workpiece, which has a negative effect on the surface quality. The simplest and most accessible variants of the melting method may be implemented with the use of electric heaters [54,55].

Arsenic sulfide (As_2S_3) and ZBLAN glass based on heavy metal fluorides (ZBLAN glasses have the ZrF_4-BaF_2-LaF_3-AlF_3-NaF composition [56]) are those materials that hold promise for mass production of mid-IR microresonators with high-quality-factor, but are still rarely used at present. They have two advantages: commercial availability in the form of optical fibers and suitable optical parameters in the middle IR range. Arsenic sulfide remains transparent up to $\sim 11\,\mu$m and has a high refraction index ($n \approx 2.4$ at a wavelength of 2 μm) and a large nonlinear coefficient ($2 \cdot 10^{-18}\,m^2/W$) [57,58]. Owing to the large nonlinear coefficient, such microresonators may be used to implement nonlinear effects [33,35,52]. ZBLAN fiber remains transparent up to $\sim 4.5\,\mu$m and has refraction index $n \approx 1.5$ within the wavelength range from 1.5 to 2.7 μm [59] and a relatively small nonlinear coefficient ($\sim 1.2 \cdot 10^{-20}\,m^2/W$ [60]). ZBLAN is readily doped with various rare earth elements and may be used to develop high-efficiency compact lasers and optical amplifiers [11,61].

In the present study, a method for production of microresonators with high-quality-factors from glasses with a relatively low (below 500°C) glass transition temperature by melting is proposed and implemented. The optimum temperature regimes for resonators made of arsenic sulfide and ZBLAN fluoride glass were determined, the causes of surface defects were investigated, and ways to prevent their formation were found. The WGM microresonator quality-factor was measured at a wavelength of 1.55 μm and found to be close to the value specified by fundamental losses in these materials. The discussed method allows one to fabricate low-loss microspheres of a given size from the above-mentioned materials quickly and reproducibly, opening up opportunities for production of microsphere-based elements for, e.g., optical sensors and microlasers.

Method of fabrication of microspherical resonators

Since the glass transition and melting temperatures of most chalcogenide and fluoride glasses vary within the 200–500°C range, the primary method for fabrication of microspherical WGM resonators from such glasses is melting. The relatively low melting point makes it somewhat easier to choose a suitable heating element. In the present study, an electric heater of a soldering station and a custom spiral heating element made of nichrome wire were used as heating elements for chalcogenide glasses based on arsenic sulfide and for fluoride glass, respectively. Figure 1 presents the overall schematic diagram of microsphere fabrication. The entire fabrication process may be divided into three key stages: fiber pre-treatment, melting, and surface quality control. The stages of fiber preparation and surface quality control of finished microspheres are the same for both materials. When preparing fiber, one needs to remove the protective polymer coating from a piece of fiber 2–3 cm in length using acetone and clean the fiber surface with lint-free wipes soaked in isopropyl alcohol to remove coating residue and other contaminants. Cleaned fiber is secured in the ferrule of a fiber connector with universal UV-curable adhesive in such a way that a fiber section 1–1.5 cm in length remains protruding. The ferrule with fiber is then placed under the heating element of the experimental setup. The heating element is lowered to the fiber workpiece and positioned at a certain distance from it; when the temperature required for melting is reached, the upper part of the fiber begins to melt, acquiring a spherical shape. During melting, the fiber shortens and shifts away from the heating element. The process of sphere formation is monitored with a microscope. Once the desired sphere diameter is reached, the heating element is pulled away from the fiber, and cooling begins. The surface of a cooled microsphere is examined with a microscope under high magnification to determine the surface quality.

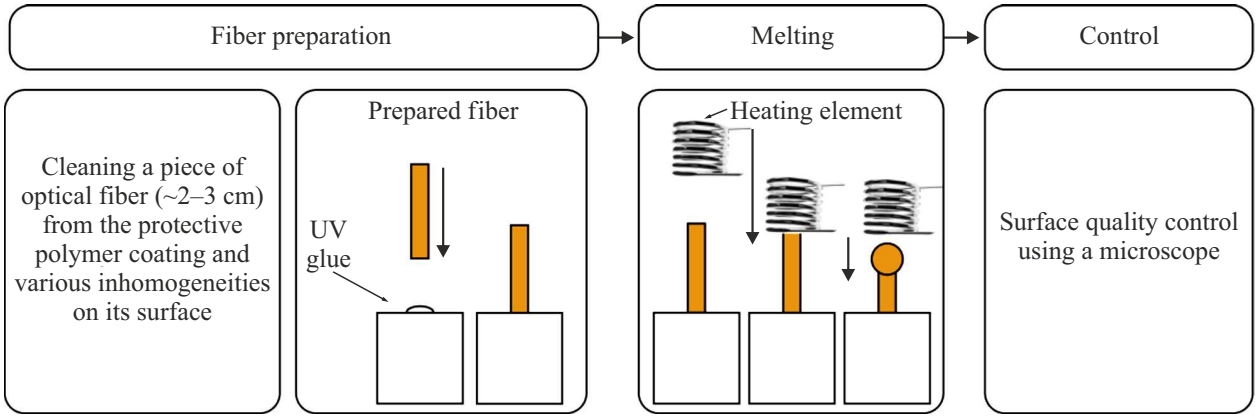

Figure 1. Diagram of fabrication of amorphous resonators from optical fiber.

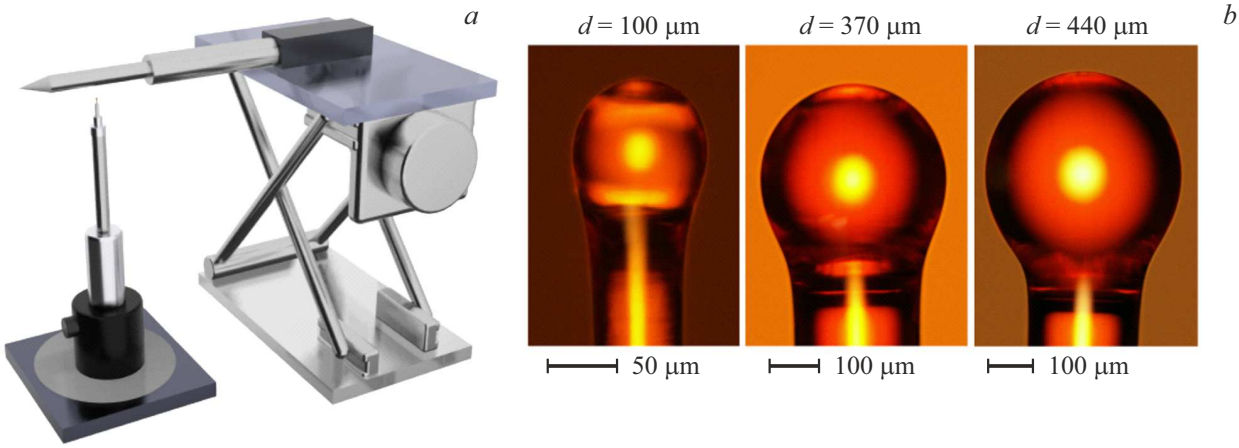

Figure 2. (*a*) Diagram of the experimental setup for fabrication of microresonators from arsenic sulfide. A soldering iron tip mounted on stage (for vertical displacement and precise alignment relative to the sphere) is used as a heating element. (*b*) Photographic image of produced arsenic sulfide microspheres with diameters of 100, 370, and 440 μm.

Commercial single-mode (6/125 μm) and multimode (12/250 μm) fibers made of arsenic sulfide (As_2S_3), which were produced at the Institute of Chemistry of High-Purity Substances of the Russian Academy of Sciences, and single-mode (9/125 μm) ZBLAN fibers based on heavy metal fluorides (with the ZrF_4-BaF_2-LaF_3-AlF_3-NaF composition), which were produced by Thorlabs, were used as the initial materials for microsphere fabrication. Their glass transition temperatures are as follows: $As_2S_3 \sim 190^\circ$C [57], ZBLAN $\sim 265^\circ$C [62].

Arsenic sulfide microresonators

Figure 2, *a* shows the experimental setup for production of microspheres from As_2S_3, where a Lukey 852D+ soldering station was used as a heating element. With the operating temperature of the heater being 230°C, the copper tip of the soldering iron is lowered using a high-precision positioner to a distance of approximately 300 μm from the fiber. Since the fiber gets shorter in the process of melting and sphere formation, one needs to lower the heating element smoothly to increase the microsphere diameter. The end diameter is monitored with a microscope during melting. This setup provides an opportunity to produce microspheres with diameters ranging from 50 to 500 μm.

Multimode As_2S_3 fiber was used to fabricate microspheres with diameters larger than 250 μm, and single-mode As_2S_3 fiber was used for microspheres with diameters of 150–250 μm.

Fiber tapering

To obtain microspheres with a diameter below 150 μm, one needs first to taper single-mode fiber until it reaches a thickness that is 20−30 μm smaller than the desired end sphere diameter. The melting method was also used to produce tapered arsenic sulfide fiber. The procedure involved heating to a temperature slightly above the glass transition temperature of the fiber with simultaneous pulling in opposite directions. Figures 3, *a* and *b* present the

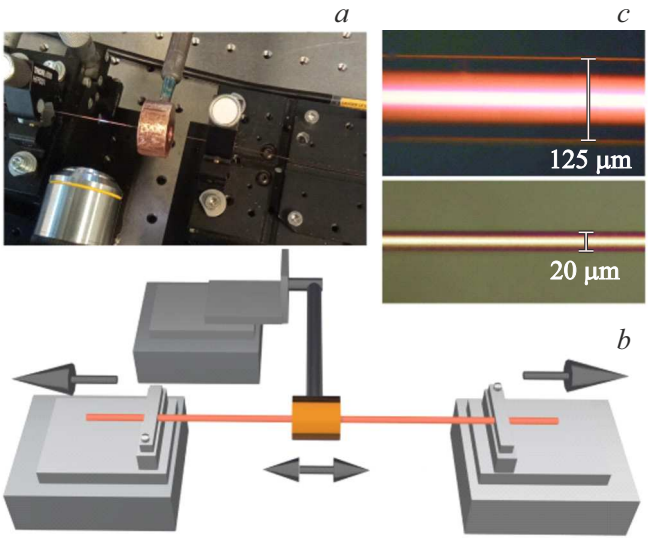

Figure 3. (*a*) Photographic image of a heating element with fiber. (*b*) Schematic diagram of the experimental setup for tapering arsenic sulfide fiber. (*c*) Photographic images of fibers before and after tapering.

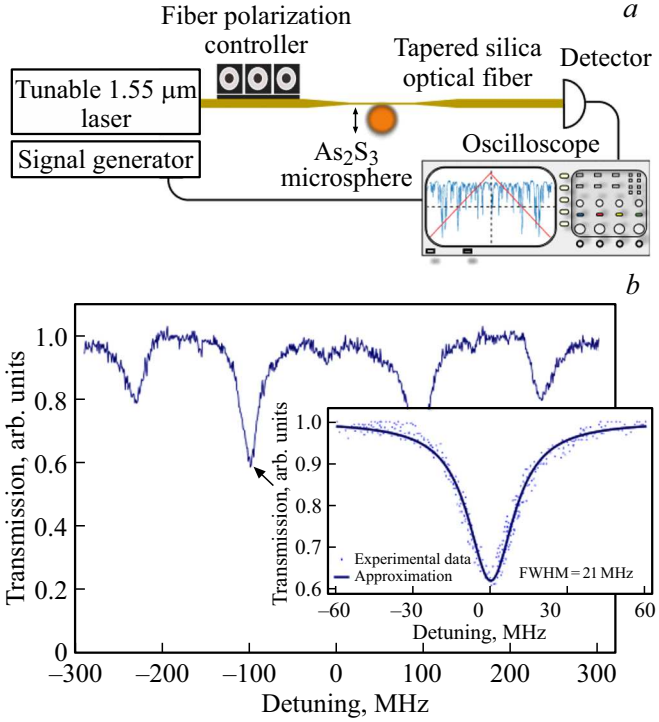

Figure 4. (*a*) Experimental setup for excitation of WGMs. (*b*) Transmission spectrum for a microsphere with a diameter of 200 μm. The resonance curve approximated by a Lorentzian function with a width of 24 MHz, which corresponds to loaded quality factor $Q = 5.1 \cdot 10^6$, is shown in the inset.

photographic image and the diagram of the fiber tapering setup. In preparation for tapering, one also needs first to remove the polymer coating from a fiber section $\sim 5-6$ cm in length and clean the surface with alcohol. The prepared workpiece is then secured on two motorized stages with fiber holders, and the cleaned fiber section is positioned inside the heating element. A split copper cylinder 1 cm in length with an outer diameter of 2 cm and a hole with a diameter of 6 mm was used as a heating element to obtain a uniform temperature distribution in the internal cavity. A constant temperature of $\sim 305^\circ$C was maintained at the center of the cylinder.

The heating element on a motorized stage performs oscillatory motion along the fiber with an amplitude of 5 mm and a speed of 15 μm/s, while the ends of fibers, which are also secured to motorized stages, shift in opposite directions at a speed of 10 μm/s. The fiber profile and thickness are monitored with a microscope. Once the required fiber thickness is reached, the heater is turned off, the motorized stages are stopped, and the heating element continues to oscillate along the fiber until the element cools completely. Figure 3, *c* shows photographic images taken before and after tapering a single-mode fiber with a thickness of 125 μm to a thickness of 20 μm. Following cooling of the heating element, the tapered fiber is divided into two at its thinnest point. Each of these two parts may be used to make microspheres.

Microspherical arsenic sulfide resonators with diameters ranging from 50 to 500 μm were obtained as a result. Figure 2, *b* shows the obtained microspheres with diameters of 100, 370, and 440 μm. To assess the quality of microspheres, one needs to determine the quality factor of manufactured resonators. The experimental setup presented in Fig. 4, *a* was used for this purpose. A tunable diode laser with a radiation wavelength of 1.55 μm was used to excite whispering gallery modes. The polarization state of laser radiation was adjusted with a polarization controller. Tapered silica fiber with a thickness up to ~ 1 μm at the waist was used as a coupling element. Tapered fiber was also used to couple radiation to a photodetector. The microsphere was positioned on a precision stage with a piezo controller. The full width at half maximum (FWHM) of the resonance curve in the transmission spectrum was measured in order to calculate the quality factor. A Mach–Zehnder interferometer with a 102 MHz free spectral range was used for frequency calibration. Due to the influence of static electricity, this coupling element is susceptible to sticking to the resonator; therefore, it does not allow one to evaluate the quality factor in the critical coupling regime, where coupling losses are equal to losses within the resonator. Figure 4, *b* shows the transmission spectrum for a microsphere with a diameter of 200 μm. The loaded resonance quality factor was $5.1 \cdot 10^6$, which is comparable to record-high values for this material [32].

ZBLAN fluoride glass microresonators

The procedure of preparation of ZBLAN fluoride fiber is virtually the same as the one described above for As_2S_3

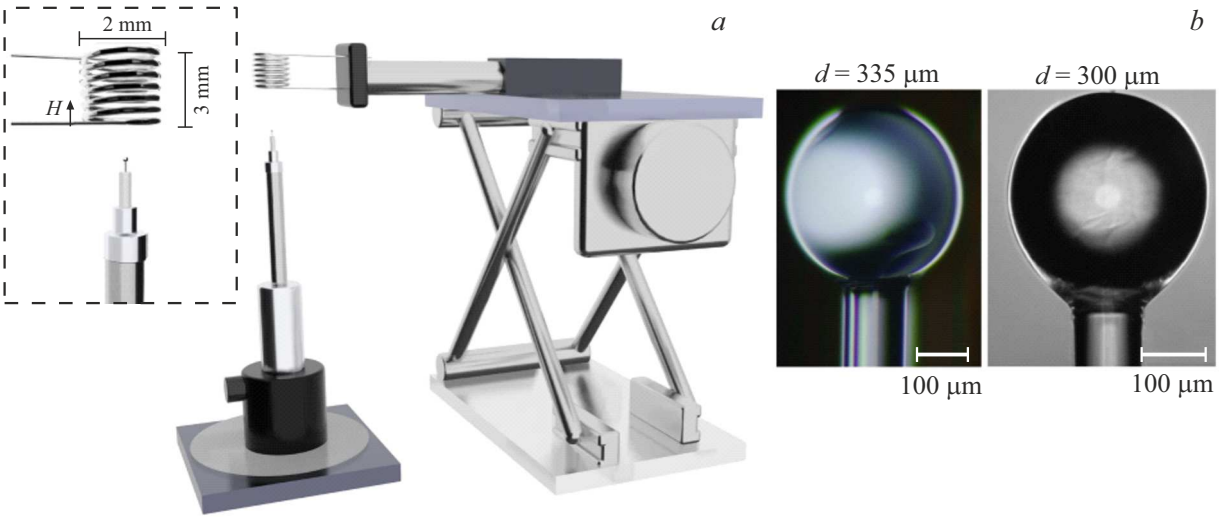

Figure 5. (*a*) Diagram of the experimental setup for fabrication of microresonators from ZBLAN fluoride glass. A nichrome wire spiral is used as a heating element. (*b*) Photographic image of produced microspheres with diameters of 300 and 335 μm.

fiber, except that the fluoride fiber has a dual layer of polymer coating, which needs to be soaked for 5 min in an acetone solution. The setup was also altered: the heating element was replaced with a nichrome wire spiral with a diameter of 2 mm and a height of 3 mm (the wire diameter was 0.16 mm) powered by a direct current source. The heating element needed to be replaced due to the fact that ZBLAN requires a more uniform temperature distribution at an optimum heating rate. Microspherical ZBLAN WGM resonators were fabricated under rapid (within 2 s) heating of the fiber to a maximum temperature of 500°C inside the heating element. A Keithley series 2220 current source with $V = 6.9$ V and $I = 1.4$ A was used to power the heating element. Two microscopes placed above and in front of the fiber workpiece and a precision three-axis stage were used to position the prepared fiber in the center of the spiral heating element at certain height H (Fig. 5, *a*).

The end diameter of microspheres depends in this case on initial height H of fiber placement inside the heating element and the initial fiber diameter. With H varying from 0.2 to 0.4 mm, one may fabricate microspheres from the used ZBLAN fiber with a thickness of 125 μm that vary in size within the range of 2–3 diameters of the fiber cladding (from 250 to 400 μm). The microsphere surface quality was inspected after cooling. Figure 5, *b* presents the photographic images of fabricated microspheres with diameters of 300 and 335 μm.

The experimental setup shown in Fig. 6, *a* was used to excite WGMs. A tunable 1.55 μm continuous wave laser diode pig-tailed with optical fiber was used as a radiation source. Having passed through the polarization controller, radiation enters free space and proceeds into the microresonator through a zinc selenide (ZnSe) prism, which served as a coupling element. The microresonator is mounted on a three-axis stage with a piezo controller. The transmitted light is collected by a photodetector. A silica

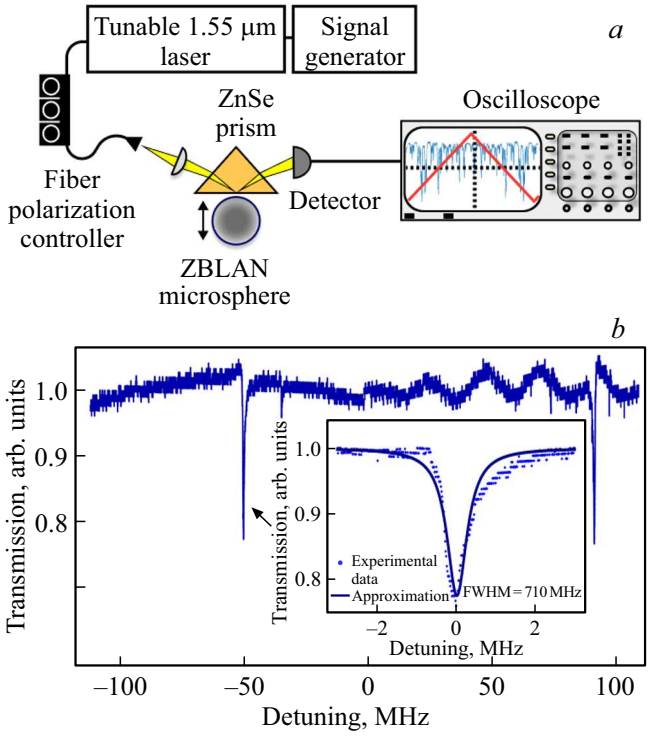

Figure 6. (*a*) Experimental setup for excitation of WGMs. (*b*) Transmission spectrum for a microsphere with a diameter of 310 μm in the critical coupling mode. The FWHM is 710 kHz, which corresponds to an unloaded quality factor of $5.4 \cdot 10^8$.

Fabry–Pérot etalon with a 1.5 GHz free spectral range was used for frequency calibration. The coupling element used allows one to adjust the loading of the microresonator by altering the distance between the resonator and the coupling element. Of particular note is the critical coupling regime established when losses due to the leakage of mode energy

into the coupling element are equal to intrinsic losses of the resonator. This mode corresponds to the deepest resonance curve in the transmission spectrum. The loaded quality factor measured in this regime provides an opportunity to estimate the intrinsic quality factor of the resonator, which is two times higher than the loaded one.

Figure 6, *b* presents the transmission spectrum for the resonator with a diameter of 310 μm. The resonance curve measured in the critical coupling regime and approximated by a Lorentzian function with a width of 710 kHz is shown in the inset. The loaded quality factor was $2.7 \cdot 10^8$. This corresponds to intrisic quality factor $Q = 5.4 \cdot 10^8$ and is a record-high level for this material. The resonance curve has the same width under forward and backward scanning of the laser radiation frequency, which is indicative of zero nonlinearity. Resonance curves of this kind are approximated by a Lorentzian function. A slight difference between the experimental resonance curve and the fitting function is the result of laser power fluctuations and spurious Fabry–Pérot resonances induced by reflection from optical elements in the experimental setup.

Specific features of fabrication of microresonators from amorphous materials

The quality factor is one of the most important parameters of WGM microresonators; therefore, the optimum fabrication method needs to be chosen to obtain microresonators with high-quality-factors. The quality factor budget generally includes material losses, radiative losses, losses associated with scattering and absorption by inhomogeneities inside and on the surface of a resonator, and coupling losses. Controlled among these are the coupling quality factor, the quality factor associated with radiative losses, and the quality factor associated with scattering on the surface. Radiative losses depend on the resonator size and are negligible for resonators with dimensions exceeding several tens of a wavelength. The coupling quality factor may be adjusted by varying the distance between the resonator and the coupling element. The surface roughness should be reduced in order to suppress losses associated with scattering on the resonator surface. To achieve this, one needs to identify all potential factors affecting negatively the surface quality in the process of fabrication and eliminate them. In the present study, the conditions of emergence of various defects on the resonator surface (associated both with the properties of the materials used and with the manufacturing process specifics) were determined in the course of fabrication. Figure 7, *a* illustrates the case of improper preparation of the fiber workpiece wherein dust particles or protective polymer coating residues get fused into the surface. This problem is easy to eliminate by cleaning the fiber surface more thoroughly with high-purity isopropyl alcohol before the melting procedure. The cases presented in Figs. 7, *b* and *c* correspond to defects forming when a proper temperature regime is not maintained during melting and cooling. An asymmetrical temperature distribution around the fiber workpiece induces deviations of the resonator shape from a spherical one and fiber bending (Fig. 7, *b*) [30,54]. Bends also form if the fiber is positioned non-vertically in the ferrule of an optical connector. Ferrules with aperture diameters of 125 and 250 μm are used for single-mode and multimode optical fibers, respectively. When the fiber is thinned, one needs to ensure that it is secured strictly vertically with universal adhesive.

Defects associated with crystallization on the resonator surface were the hardest to eliminate. The multicomponent composition of the used ZBLAN fluoride fiber aggravates the situation further. A more pronounced tendency to crystallization of a material may have a profound negative effect on the surface quality of a cooling sphere (Fig. 7, *c*). The glass-forming ability of a material depends on the resistance of glass to crystallization upon cooling within the range between the melting point and the crystallization temperature. The difference between these temperature values for the fibers used here is relatively small: the crystallization temperature varies within the 350–400°C (ZBLAN) range, and the melting temperature is $\sim$ 450°C (ZBLAN). It was demonstrated experimentally in [63] that the temperature of the onset of crystallization depends on the rates of heating and cooling of glass, allowing one to choose the optimum rate to suppress crystallization.

Two types of heating elements (a common soldering station and a spiral heating element made of nichrome wire) were used in the present study. In experiments with arsenic sulfide fibers and the soldering station, the problem with crystallization during cooling was solved easily by adjusting the rate of shifting the heating element away from the microsphere after melting. In the case of arsenic sulfide, the problem with crystallization on the surface was manifested only in the process of tapering the fibers (Fig. 7, *c*), which became unusable as a preform for microspheres. One needs to adjust the temperature smoothly as the fiber gets thinner during melting. In the present case, this was done by increasing the translational speed of the motorized stage with the heating element from 15 to 30–40 μm/s.

Having replaced the fiber with the fluoride one, we failed to find the optimum temperature regime in experiments with the soldering station. A spiral heating element was fabricated from nichrome wire to obtain a symmetrical temperature distribution inside the heating element and control the heating and cooling rates. An additional microscope installed above the heating element was also used for convenience of positioning the fiber relative to the center of the heating element. The optimum parameters, which helped eliminate all the above-mentioned factors leading to microsphere surface deformation, were then determined via step-by-step experimental adjustment of temperature and heating duration values. With these parameters set, this method provides fine reproducibility with a high quality of surfaces of the fabricated microspheres.

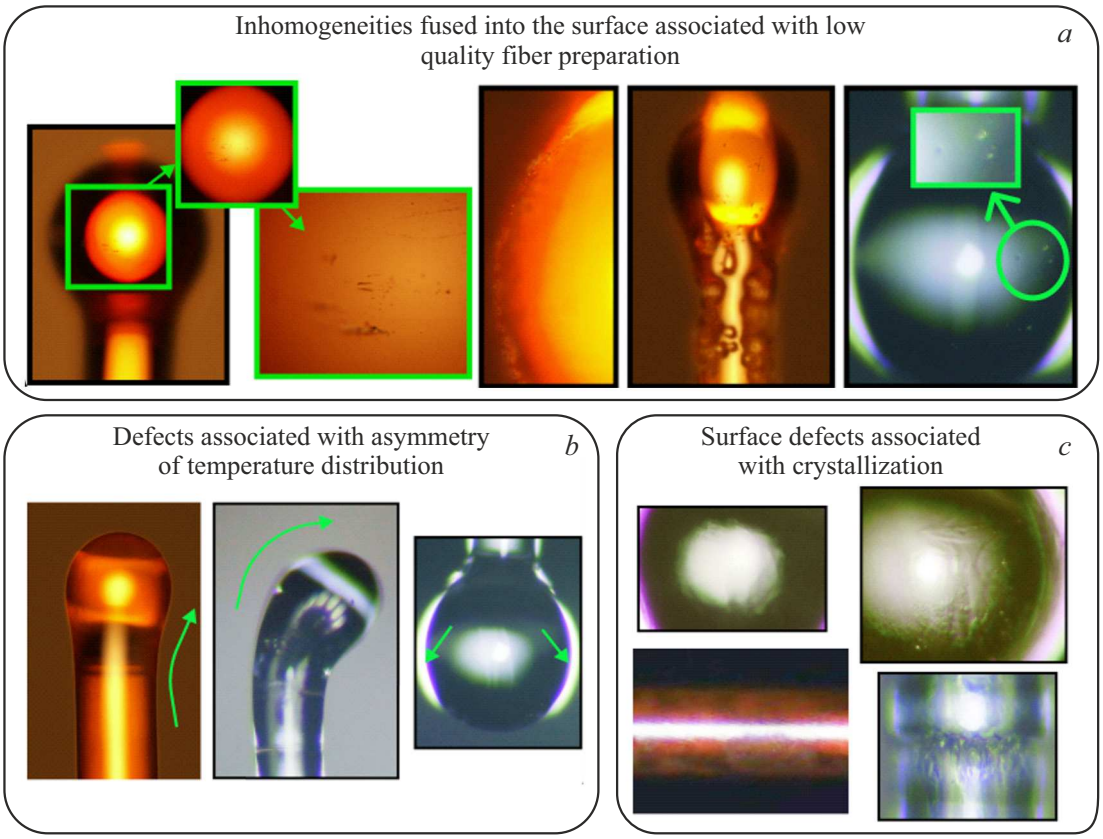

Figure 7. (a) Defects associated with inhomogeneities present on the fiber surface before melting. (b) Defects associated with the asymmetry of temperature distribution. (c) Defects associated with crystallization.

Conclusion

The process of fabrication of microspherical WGM resonators with high-quality-factors from arsenic sulfide fibers 50–500 μm in diameter and ZBLAN fluoride glass fibers 250–400 μm in diameter was demonstrated. The factors potentially inducing the formation of defects on the surface of resonators in the course of fabrication and the ways to minimize their influence were discussed. The presented method ensures fine reproducibility of parameters of the resulting microresonators combined with a high quality of surfaces of the fabricated microspheres. It provides an opportunity to reach a quality factor of microresonators comparable to record-high values for the materials used. The advantages of this method are its relative simplicity and high production rate: the entire process of fabrication of a single microsphere (from preliminary preparation of the fiber to a finished microsphere) takes approximately 10 min.

Funding

This study was supported financially by the Russian Foundation for Basic Research as part of scientific project No. 20-32-90184.

Conflict of interest

The authors declare that they have no conflict of interest.

References

[1] V.B. Braginsky, M.L. Gorodetsky, V.S. Ilchenko. Phys. Lett. A, **137**, 393–397 (1989). DOI: 10.1016/0375-9601(89)90912-2
[2] K.J. Vahala. Nature, **424**, 839–846 (2003). DOI: 10.1038/nature01939
[3] V.S. Ilchenko, A.B. Matsko. IEEE J. Select. Topics Quantum Electron., **12**, 15–32 (2006). DOI: 10.1109/JSTQE.2005.862943
[4] J. Zhu, S.K. Ozdemir, Y.-F. Xiao, L. Li, L. He, D.-R. Chen, L. Yang. Nature Photonics, **4**, 46–49 (2010). DOI: 10.1038/nphoton.2009.237
[5] J. Ward, O. Benson. Laser & Photonics Reviews **5**, 553–570 (2011). DOI: 10.1002/lpor.201000025
[6] F. Vollmer, S. Arnold. Nature Methods **5**, 591–596 (2008). DOI: 10.1038/nmeth.1221.
[7] F. Vollmer, H.G.L. Schwefel. Eur. Phys. J. Spec. Top. **223**, 1907–1916 (2014). DOI: 10.1140/epjst/e2014-02271-2
[8] G. Lin, A. Coillet, Y.K. Chembo. Adv. Opt. Photon., AOP **9**, 828–890 (2017). DOI: 10.1364/AOP.9.000828
[9] T. Kippenberg. *Nonlinear Optics in Ultra-high-Q Whispering-Gallery Optical Microcavities*, Ph.D thesis, California Institute of Technology, 2004. URL: https://thesis.library.caltech.edu/2487/.

[11] A. Pasquazi, M. Peccianti, L. Razzari, D.J. Moss, S. Coen, M. Erkintalo, Y.K. Chembo, T. Hansson, S. Wabnitz, P. Del'Haye, X. Xue, A.M. Weiner, R. Morandotti. Physics Reports **729**, 1–81 (2018). DOI: 10.1016/j.physrep.2017.08.004
[11] Y. Deng, R.K. Jain, M. Hossein-Zadeh. Optics Lett., **39**, 4458 (2014). DOI: 10.1364/OL.39.004458
[12] B. Behzadi, R.K. Jain, M. Hossein-Zadeh. Laser Physics Lett., **15**, 085112 (2018). DOI: 10.1088/1612-202X/aac5c8
[13] L. He, Ş.K. Özdemir, L. Yang, Laser & Photonics Reviews **7**, 60–82 (2013). DOI: 10.1002/lpor.201100032
[14] R.R. Galiev, N.G. Pavlov, N.M. Kondratiev, S. Koptyaev, V.E. Lobanov, A.S. Voloshin, A.S. Gorodnitskiy, M.L. Gorodetsky. Opt. Express, OE **26**, 30509–30522 (2018). DOI: 10.1364/OE.26.030509
[15] W. Liang, V.S. Ilchenko, D. Eliyahu, A.A. Savchenkov, A.B. Matsko, D. Seidel, L. Maleki. Nature Communications **6**, 7371 (2015). DOI: 10.1038/ncomms8371
[16] A.E. Shitikov, I.I. Lykov, O.V. Benderov, D.A. Chermoshentsev, I.K. Gorelov, A.N. Danilin, R.R. Galiev, N.M. Kondratiev, S.J. Cordette, A.V. Rodin, A.V. Masalov, V.E. Lobanov, I.A. Bilenko, Opt. Express, **31**, 313–327 (2023). DOI: 10.1364/OE.478009
[17] S. Arnold, D. Keng, S.I. Shopova, S. Holler, W. Zurawsky, F. Vollmer. Opt. Express **17**, 6230 (2009). DOI: 10.1364/OE.17.006230
[18] W. von Klitzing, R. Long, V.S. Ilchenko, J. Hare, V. Lefèvre-Seguin. New J. Phys. **3**, 14–14 (2001). DOI: 10.1088/1367-2630/3/1/314
[19] B. Behzadi, R.K. Jain, M. Hossein-Zadeh. IEEE J. Quantum Electron., **53**, 1–9 (2017). DOI: 10.1109/JQE.2017.2771423
[20] S. Jiang, C. Guo, K. Che, Z. Luo, T. Du, H. Fu, H. Xu, Z. Cai. Photon. Res., **7**, 566–572 (2019). DOI: 10.1364/PRJ.7.000566
[21] A.E. Shitikov, I.A. Bilenko, N.M. Kondratiev, V.E. Lobanov, A. Markosyan, M.L. Gorodetsky. Optica, **5**, 1525–1528 (2018). DOI: 10.1364/OPTICA.5.001525
[22] R. Shankar, I. Bulu, M. Lončar. Applied Physics Lett. **102**, 051108 (2013). DOI: 10.1063/1.4791558
[23] D. Ren, C. Dong, S.J. Addamane, D. Burghoff. Nature Communications **13**, 5727 (2022). DOI: 10.1038/s41467-022-32706-1
[24] R. Armand, M. Perestjuk, A. Della Torre, M. Sinobad, A. Mitchell, A. Boes, J.-M. Hartmann, J.-M. Fedeli, V. Reboud, P. Brianceau, A. De Rossi, S. Combrié, C. Monat, C. Grillet. APL Photonics, **8**, 071301 (2023). DOI: 10.1063/5.0149324
[25] T.-H. Xiao, Z. Zhao, W. Zhou, C.-Y. Chang, S.Y. Set, M. Takenaka, H.K. Tsang, Z. Cheng, K. Goda. Opt. Lett., **43**, 2885 (2018). DOI: 10.1364/OL.43.002885
[26] P. Wang, T. Lee, M. Ding, A. Dhar, T. Hawkins, P. Foy, Y. Semenova, Q. Wu, J. Sahu, G. Farrell, J. Ballato, G. Brambilla. Opt. Lett., **37**, 728 (2012). DOI: 10.1364/OL.37.000728
[27] I.S. Grudinin, K. Mansour, N. Yu. Opt. Lett., **41**, 2378 (2016). DOI: 10.1364/OL.41.002378
[28] W. Liang, A.B. Matsko, A.A. Savchenkov, V.S. Ilchenko, D. Seidel, L. Maleki, In: 2011 Joint Conference of the IEEE International Frequency Control and the European Frequency and Time Forum (FCS) Proceedings, p. 1–6. DOI: 10.1109/FCS.2011.5977304
[29] C. Lecaplain, C. Javerzac-Galy, M.L. Gorodetsky, T.J. Kippenberg. Nature Communications, **7**, 13383 (2016). DOI: 10.1038/ncomms13383
[30] B. Way, R.K. Jain, M. Hossein-Zadeh. In: IEEE Photonics Conference 2012, p. 143–144.
[31] R.K. Jain, B. Way, M. Klopfer, I. Small, M. Saad, M. Hossein-Zadeh. In: IEEE Photonics Conference 2012, p. 727–728.
[32] F. Vanier, P. Bianucci, N. Godbout, M. Rochette, Y.-A. Peter. In: *2012 International Conference on Optical MEMS and Nanophotonics* (2012), p. 45–46.
[33] A.V. Andrianov, E.A. Anashkina. Opt. Express, OE **29**, 5580–5587 (2021). DOI: 10.1364/OE.415787
[34] E.A. Anashkina, A.A. Sorokin, M.P. Marisova, A.V. Andrianov. J. Non-Crystalline Solids, **522**, 119567 (2019). DOI: 10.1016/j.jnoncrysol.2019.119567
[35] F. Vanier. *Nonlinear optics in chalcogenide and tellurite microspheres for the generation of mid-infrared frequencies*, Ph.D. thesis, École Polytechnique de Montréal, 2015. URL: https://publications.polymtl.ca/2021/
[36] V.S. Ilchenko, A.A. Savchenkov, A.B. Matsko, L. Maleki. Phys. Rev. Lett., **92**, 043903 (2004). DOI: 10.1103/PhysRevLett.92.043903
[37] K.N. Minkov, A.N. Danilin, A.E. Shitikov, I.K. Gorelov, M.L. Galkin, A.V. Mantuzov, E.A. Artemov, M.I. Krasivskaya, V.E. Lobanov, I.A. Bilenko. J. Opt. Technol., **89**, 691 (2022). DOI: 10.1364/JOT.89.000691
[38] K.N. Min'kov, G.V. Likhachev, N.G. Pavlov, A.N. Danilin, A.E. Shitikov, A.I. Yurin, E.A. Lonshakov, F.V. Bulygin, V.E. Lobanov, I.A. Bilenko. J. Opt. Technol., **88**, 348 (2021). DOI: 10.1364/JOT.88.000348
[39] M.L. Gorodetsky, A.A. Savchenkov, V.S. Ilchenko. Optics Lett., **21**, 453–455 (1996). DOI: 10.1364/OL.21.000453
[40] J.M. Ward, Y. Wu, K. Khalfi, S.N. Chormaic. Review of Scientific Instruments, **81**, 073106 (2010). DOI: 10.1063/1.3455198
[41] G.R. Elliott, G.S. Murugan, J.S. Wilkinson, M.N. Zervas, D.W. Hewak. Opt. Express, OE **18**, 26720–26727 (2010). DOI: 10.1364/OE.18.026720
[42] Y. Xie, D. Cai, J. Pan, N. Zhou, Y. Gao, Y. Jin, X. Jiang, J. Qiu, P. Wang, X. Guo, L. Tong. Small, **17**, 2100140 (2021). DOI: 10.1002/smll.202100140
[43] D. O'Shea, C. Junge, S. Nickel, M. Pöllinger, A. Rauschenbeutel. In: *Laser Resonators and Beam Control XIII* (International Society for Optics and Photonics, 2011), vol. 7913, p. 79130N.
[44] G.S. Murugan, J.S. Wilkinson, M.N. Zervas. Opt. Express, OE **17**, 11916–11925 (2009). DOI: 10.1364/OE.17.011916
[45] S.B. Papp, P. Del'Haye, S.A. Diddams. Phys. Rev. X, **3**, 031003 (2013). DOI: 10.1103/PhysRevX.3.031003
[46] P. Del'Haye, S.A. Diddams, S.B. Papp. Appl. Phys. Lett., **102**, 221119 (2013). DOI: 10.1063/1.4809781
[47] M. Sumetsky, J.M. Fini. Opt. Express, OE **19**, 26470–26485 (2011). DOI: 10.1364/OE.19.026470
[48] M. Sumetsky. Progress in Quantum Electronics, **64**, 1–30 (2019). DOI: 10.1016/j.pquantelec.2019.04.001
[49] N.A. Toropov, M. Sumetsky. Opt. Lett., **41**, 2278 (2016). DOI: 10.1364/OL.41.002278.
[50] M. Sumetsky, Y. Dulashko. Opt. Express, OE **20**, 27896–27901 (2012). DOI: 10.1364/OE.20.027896
[51] F. Vanier, M. Rochette, N. Godbout, Y.-A. Peter. Opt. Lett., OL **38**, 4966–4969 (2013). DOI: 10.1364/OL.38.004966
[52] F. Vanier, Y.-A. Peter, M. Rochette. Opt. Express, OE **22**, 28731–28739 (2014). DOI: 10.1364/OE.22.028731
[53] D.K. Armani, T.J. Kippenberg, S.M. Spillane, K.J. Vahala. Nature, **421**, 925–928 (2003). DOI: 10.1038/nature01371
[54] B. Way, R.K. Jain, M. Hossein-Zadeh. Opt. Lett., OL **37**, 4389–4391 (2012). DOI: 10.1364/OL.37.004389
[55] P. Wang, G.S. Murugan, G. Brambilla, M. Ding, Y. Semenova, Q. Wu, G. Farrel. IEEE Photonics Technology Lett., **24**, 1103–

1105 (2012). DOI: 10.1109/LPT.2012.2195722
[56] M. Poulain, M. Poulain, J. Lucas. Materials Research Bulletin **10**, 243–246 (1975). DOI: 10.1016/0025-5408(75)90106-3
[57] L.V. Zhukova, A.S. Korsakov, A.E. L'vov, D.D. Salimgareev. *Volokonnye svetovody dlya srednego infrakrasnogo diapazona* (Ekaterinburg, Uchebno-Metod. Tsentr UPI, 2016) (in Russian).
[58] B.J. Eggleton. Opt. Express, OE **18**, 26632–26634 (2010). DOI: 10.1364/OE.18.026632
[59] L. Zhang, F. Gan, P. Wang. Appl. Opt., AO **33**, 50–56 (1994). DOI: 10.1364/AO.33.000050
[60] E.A. Anashkina. *Dispersionnye i nelineinye svoistva sfericheskikh mikrorezonatorov na osnove razlichnykh stekol* (Nizhny Novgorod, Nizhegorod. Gos. Univ., 2019) (in Russian).
[61] L. Wetenkamp, G.F. West, H. Többen. J. Non-Crystalline Solids, **140**, 35–40 (1992). DOI: 10.1016/S0022-3093(05)80737-9
[62] L.A. Harrington. *Infrared Fibers and Their Applications* (SPIE Press, 2004).
[63] T.-C. Ong, B. Fogarty, T. Steinberg, E. Jaatinen, J. Bell. International Journal of Applied Glass Science, **10**, 391–400 (2019). DOI: 10.1111/ijag.13096

Translated by D.Safin